

# Performance of Parameter Estimation from UWB-IR Signals with an Array of Orthonormal Correlators

Giuseppe Thadeu Freitas de Abreu,  
giuseppe@ee.oulu.fi

Center for Wireless Communications, University of Oulu  
P.O. box 4500, 90014-Oulu, Finland

**Abstract**—The performance of a method for the estimation of physical parameters from impulsive waveforms utilizing an array of correlators is studied through Cramer-Rao lower bound analysis. The analysis is made possible by the introduction of a Hermite wavelet model for the impulsive signals. Exploiting the existence of closed-form correlation formulae of Hermite wavelets, the problem of parameter estimation from ultra wideband (UWB) impulse-radio signals is brought to conditions similar to those found in conventional narrow-band array signal processing, and yielding a mathematical mathematically tractable description of the output of the array of correlators. Numerical examples exploring the influences of the array topology and template waveform design on the estimation accuracies of angle of arrival and time difference of arrival are also provided.

## I. INTRODUCTION

The estimation of physical parameters such as signal strength, time difference of arrival (TDoA) and angles of arrival (AoA) for beamforming, ranging, positioning and channel sounding applications is a classic problem in the area of array signal processing. In the special case of parameter estimation from wideband signals, this problem has generally been addressed by transforming the output of the array into a set of separate vectors each preserving a portion of the information on the spatial, temporal and frequency characteristics of the impinging waveforms [1]–[3]. Unfortunately, this “classic” decomposition approach requires the manipulation of a number of variables many times larger than that of parameters to be estimated, leading to algorithms whose complexities increase manyfold with the bandwidth of the signals.

For chirp waveforms, in which an increase in the bandwidth of the signal results in a proportional increase in the symbol duration, the classic wideband approach is still applicable as shown in [4], [5]. The bandwidth of impulsive waveforms, on the other hand, is associated with a shorter symbol duration, rendering approaches based on time or frequency domain decomposition unrealistic for impulsive UWB signals. Non-surprisingly, contributions in the area of UWB array antennas are rare and, to the best of our knowledge, limited to beamforming techniques [6], [7]. Although the AoA of UWB impulses could be extracted from the structure of corresponding steering vectors, the inaccuracy of such an approach can be inferred from a parallel with the narrowband case [8], and has led to the perception that array signal processing techniques are not applicable for UWB impulsive signals [9].

It is known that the Hermite polynomials are energy eigenfunctions of the Harmonic oscillator, such that the waveforms naturally arising from near-equilibrium oscillatory processes are Hermite wavelets [10]. Consequently, the waveforms produced by state-of-the-art UWB pulse-generators [11], [12] are

accurately modeled by Hermite functions [13].

It has been recently shown that this model can be exploited to devise a theory that enables the application of narrowband array signal processing to the analysis of UWB signals [14]. Examples of the implementation of the Capon beamformer and the MUSIC algorithm to the estimation of TDoA and DoA were provided in [14]. In this paper, we add to that contribution by providing a more general and theoretical evidence of the efficacy of that approach. The remainder of the paper is as follows. In section II, the mathematical model for the UWB impulsive signals and fundamental aspects of the array receiver structure and described. The structure of the bank of correlators employed across the array in order to bring the problem of parameter estimation of UWB signals to narrowband-like conditions is briefly revised in section III. The Cramer-Rao lower bound analysis on the variances of the estimation errors associated to the physical parameters is carried out in section IV.

## II. SIGNAL MODEL AND ARRAY STRUCTURE

A common definition of Hermite wavelets is given by [15]

$$\psi_n(t) \triangleq \frac{H_n(t)e^{-\frac{t^2}{2}}}{\sqrt{2^n n! \sqrt{\pi}}}, \quad (1)$$

where  $H_n(t)$  are the Hermite polynomials defined by<sup>1</sup>

$$H_n(t) \triangleq (-1)^n e^{t^2} \frac{d^n}{dt^n} e^{-t^2} \quad n \in \mathbb{N}. \quad (2)$$

Let us denote the Euclidian distance from the  $n$ -th element to the center of an array immersed in an isotropic medium by  $d_n$  and, without loss of generality, label the antennas such that  $d_{N-1}$  gives the array’s largest dimension.

In order to ensure that all  $N$  elements of array receiving a given pulse “sample” the same waveform,  $d_{N-1}$  must satisfy

$$d_{N-1} \leq cT = \lambda, \quad (3)$$

where  $T$  is the time taken by a single impulse to propagate in the medium with speed  $c$ .

The product  $\lambda = cT$  gives the length (in meters) of  $\psi_n(t)$  and, therefore, is hereafter referred to as the *wavelength* of the pulse. Note that the condition described by equation (3) does not result in unrealistic requirements on the size of the array receiver. For example, for  $T = 250$ ps, which is short enough to allow full multipath resolvability [17], it is found that  $d_{N-1}$  is upper-bounded by the rather large figure of 7.5cm.

<sup>1</sup>A more general definition of Hermite wavelet and closed form formulae for the corresponding correlation functions can be found in [16].

Let  $K$  impulses, each modeled as a Hermite function of  $m_k$ -th order with amplitude  $\gamma_k^2$  and bearing the symbol  $s_k$ , impinge onto the array from the direction described by the pair of angles  $(\theta_k, \phi_k)$ . Then, the TDoA of the  $k$ -th pulse at the  $n$ -th element relative to an arbitrary reference becomes:

$$\Delta\tau_{k,n} = -\frac{d_n}{c} \cos(\theta_k - \vartheta_n) \cos(\phi_k - \varphi_n), \quad (4)$$

where  $(d_n, \vartheta_n, \varphi_n)$  are the cylindric coordinates of the  $n$ -th element, with respect to the reference.

Let the signal received at the  $n$ -th element be correlated against a template wavelet  $\xi_n(t)$ , and denote the TDoA of the  $k$ -th signal by  $\tau_k$ . Then, the array output in the presence of the  $k$ -th signal is given by

$$\mathbf{a}_k = [R_{0,m_k}(\tau_k) \cdots R_{N-1,m_k}(\tau_k + \Delta\tau_{k,N-1})]^T, \quad (5)$$

where  $^T$  denotes transpose,  $R_{n,m}(\tau)$  is the correlation function of the template and impinging waveforms  $\xi_n(t)$  and  $\psi_m(t)$ .

Form all the above, the array output in the presence of all  $K$  signals, interference and noise, in a stationary scenario is

$$\mathbf{r} = \sum_{k=0}^{N-1} (\mathbf{a}_k \gamma_k s_k) + \mathbf{w} = \mathbf{A} \cdot \mathbf{\Gamma} \cdot \mathbf{s} + \mathbf{w}, \quad (6)$$

where the pulse amplitude matrix  $\mathbf{\Gamma}$ , the array manifold matrix  $\mathbf{A}$ , the symbol vector  $\mathbf{s}$ , and the noise vector  $\mathbf{w}$  are all real-valued quantities respectively given by

$$\mathbf{A} = [\mathbf{a}_0 \ \mathbf{a}_1 \ \cdots \ \mathbf{a}_{K-1}], \quad (7)$$

$$\mathbf{\Gamma} = \begin{bmatrix} \gamma_0 & & \mathbf{0} \\ \mathbf{0} & \ddots & \\ & & \gamma_{K-1} \end{bmatrix}, \quad (8)$$

$$\mathbf{s} = [s_0 \ s_1 \ \cdots \ s_{K-1}]^T, \quad (9)$$

$$\mathbf{w} = [w_0 \ w_1 \ \cdots \ w_{N-1}]^T. \quad (10)$$

The similarity between the structure of the array receive vector given by equation (6) and that found in the narrowband array signal processing literature [8] is evident.

Many of the high-resolution parameter estimation techniques of relative lower complexity rely on moments of the array output vector, such as the covariance matrix (second-order moment) or the cumulant matrix (fourth-order moments) [18]. These techniques are known to be sensitive to correlation amongst the entries of the noise vector, to non-Gaussianity of the randoms, and to the distribution of the noise powers across the array [18]–[20]

Fortunately, the central limit theorem ensures that  $w_n$  have Gaussian statistics [17] and a classic communication-theoretic result on the correlation receiver [21] establishes that if the correlation filters used at different antenna elements have unitary energy and are orthogonal to one another,  $w_n$  are independent and identically distributed (i.i.d.) processes. Furthermore, the fact that UWB correlators are essentially ultra-wide passband filters implies that the spectra of  $w_n$  are approximately white.

It is understood from the above arguments that if the correlation templates  $\xi_n(t)$  are orthonormal functions, the noise vector  $\mathbf{w}$  can be modeled as a sample vector of real, additive white Gaussian (AWG), independent and identically distributed (i.i.d.) randoms of zero mean and variance  $\sigma_w^2$ , reproducing the conditions generally observed (or assumed) for the noise vector in narrowband array signal processing techniques. In other words, an expedient choice of template wavelets  $\xi_n(t)$  leads to a noise covariance and array covariance matrices respectively given by

$$\mathbf{R}_w = \mathbb{E}[\mathbf{w} \cdot \mathbf{w}^T] = \sigma_w^2 \mathbf{I}, \quad (11)$$

$$\mathbf{R} = \mathbb{E}[\mathbf{r} \cdot \mathbf{r}^T] = \mathbf{A} \cdot \mathbf{\Gamma} \cdot \mathbf{R}_s \cdot \mathbf{\Gamma}^T \cdot \mathbf{A}^T + \sigma_w^2 \mathbf{I}. \quad (12)$$

where  $\mathbb{E}[\ ]$  denotes expectation,  $\mathbf{I}$  is the identity matrix, and  $\mathbf{R}_s$  is the signal covariance matrix.

### III. CONSTRUCTION OF THE CORRELATORS

A natural choice for the orthonormal template wavelets  $\xi_n(t)$  to be used at the antenna elements are the Hermite wavelets, as defined in equation (1). A closed-form expression for the correlation function of any arbitrary pair  $(n, m)$  of Hermite wavelets is given by [22]

$$R_{n,m}(\tau) = \frac{(-1)^{2m+n} \sqrt{n!m!}}{\sqrt{2^{n+m}} e^{\frac{\tau^2}{4}}} \sum_{k=0}^{\lfloor (n,m) \rfloor} (-2)^k \tau^{n+m/2k} (n-k)!(m-k)!k!, \quad (13)$$

where  $\lfloor (n, m) \rfloor$  denotes the minimum between the pair  $(n, m)$ .

Unfortunately, the use of Hermite orthogonal filters at the array may lead to situations where the output of the correlators not matched to the impinging waveforms are negligible, significantly reducing the degrees of freedom of the receiver. For instance, the response of a uniform linear array (ULA) to a perfectly synchronized distortionless impulse impinging from broadside would be a vector with a single non-zero output!

This problem can be solved by generalizing the array construction, such that the correlation templates are given by combinations of Hermite wavelets, that is,

$$\xi_n(t) = \frac{1}{Q} \sum_{q=0}^{Q-1} b_{n,q} \psi_q(t). \quad (14)$$

The cross-correlation functions of the template wavelets  $\xi_n(t)$  and the Hermite UWB waveforms  $\psi_m(t)$  can be easily obtained from equations (14) and (15), yielding

$$\tilde{R}_{n,m}(\tau) = \int_{-\infty}^{\infty} \xi_n(t) \psi_m(t - \tau) dt = \frac{1}{Q} \sum_{q=0}^{Q-1} b_{n,q} R_{q,m}(\tau). \quad (15)$$

It follows that the array output corresponding to the  $k$ -th source is given by

$$\tilde{\mathbf{a}}_k = \text{diag}\{\mathbf{B} \cdot \tilde{\mathbf{R}}_k\} / Q, \quad (16)$$

where the  $N$ -by- $Q$  matrix  $\mathbf{B}$  is build from the coefficient entries  $b_{n,q}$ , and  $\tilde{\mathbf{R}}_k$  is a  $Q$ -by- $N$  matrix carrying the projections of the UWB waveform arriving at each antenna, over the basis of the Hermite subspace of dimension  $Q$ , which is given by

$$\tilde{\mathbf{R}}_k = \begin{bmatrix} R_{0,m_k}(\tau_k) & \cdots & R_{0,m_k}(\tau_k + \Delta\tau_{k,N-1}) \\ \vdots & \ddots & \vdots \\ R_{Q-1,m_k}(\tau_k) & \cdots & R_{Q-1,m_k}(\tau_k + \Delta\tau_{k,N-1}) \end{bmatrix}. \quad (17)$$

Orthogonality, transmit power limitation and complexity constraints lead to a Hermite-Hadamard construction<sup>2</sup> for the coefficient matrix  $\mathbf{B}$ . The Hermite-Hadamard construction results in an even distribution of the energy collected across the elements of the array subject to the presence of an incoming UWB signal. This is graphically described by the following quantity, referred to as the *apparent size* of the array:

$$\Sigma_{\mathbf{B}_i}(\tilde{\tau}) \triangleq \frac{1}{\max(|\tilde{a}_n(\tilde{\tau})|)} \sum_{n=0}^{N-1} |\tilde{a}_n(\tilde{\tau})|, \quad (18)$$

where  $\tilde{\tau} = \tau + \Delta\tau$  combines the effects of  $\tau$ ,  $\theta$  and  $\phi$ .

<sup>2</sup>Details can be found in [14].

Given a certain direction of arrival  $\tilde{\tau}$ , the apparent size  $\Sigma_{\mathbf{B}_i}$  approaches  $N$  when the absolute value of the output of all elements are non-zero and equal to one another, and decreases if any of the antenna elements collects a larger amount of energy than all the others or if any of the elements have a null output. In other words,  $\Sigma_{\mathbf{B}_i}$  gives us an idea of the number of elements in the array that are effectively useful in sampling the signal arriving from the locus  $\tilde{\tau}$ , defined by the parameters  $\tau$ ,  $\theta$  and  $\phi$ .

Since a large number of distinct partitioned permutations of the Hadamard matrix can be constructed, the apparent array size is dependent on the particular choice of coefficient matrix  $\mathbf{B}_i$ , as indicated by the notation. This gives us a practical method to optimize the coefficient matrix, namely, select the coefficient matrices  $\mathbf{B}_i$  that results in the apparent array size curve that is closest to the *envelope* of all such curves obtained with all possible mutually exclusive  $\mathbf{B}_i$ , denoted by  $[\Sigma_{\mathbb{B}}(\theta)]$ . Figure 1 provides a few examples of  $\Sigma_{\mathbf{B}_i}$  for different  $\mathbf{B}_i$ , together with their envelope  $[\Sigma_{\mathbb{B}}(\theta)]$ .

While the comparison between  $\Sigma_{\mathbf{B}_i}(\tilde{\tau})$  and  $[\Sigma_{\mathbb{B}}(\theta)]$  needs be, in principle, performed over  $\tilde{\tau}$ , it will be latter shown that the Cramer-Rao bound on the variance of the TDoA estimates  $\hat{\tau}$  are significantly lower than those for the angle parameters  $\hat{\theta}$  and  $\hat{\phi}$ , such that the optimization of  $\mathbf{B}_i$  can be performed over the spatial domain only, which simplifies the procedure.

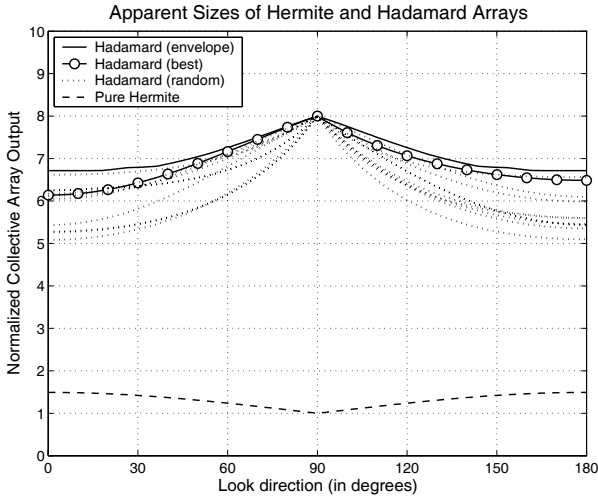


Fig. 1. Uniform Linear Array ( $N = Q = 8$ ; Length  $\lambda$ ).

#### IV. CRAMER-RAO BOUNDS

While examples of the implemented well-known narrow-band array signal processing techniques to the estimation of location parameters directly from UWB signals using the theory here introduced were given in [14], it is important to assess the performance of the approach from a more general and theoretical point of view. For that matter, it is of special interest to quantify the relative performances of the Hermite and the Hadamard arrays discussed in section II and III, from a standpoint independent of particular estimation algorithms. This can be achieved by computing the Cramer-Rao bound on the variance of the estimation errors associated to the physical parameters that describe the receive vector  $\mathbf{r}$  and the array covariance matrix  $\mathbf{R}$  (see equations (6) and (12)), which can be grouped in a vector parameter  $\boldsymbol{\eta} = \{\sigma_w^2, \gamma, \tau, \theta, \phi\}$ .

If the transmit symbols are bipolar, the stationarity of the scenario and the noise Gaussianity imply that the error vectors are samples of a Gaussian zero-mean stochastic process. Although this assumption is not generally satisfied, it has been shown that this assumption results in a maximization of the Cramer-Rao bound [23], leading to a conservative prediction of the estimation performance, which inflicts no harm on the results of the analysis.

Under the Gaussian assumption, the likelihood function of the data becomes [24]

$$\mathbf{L}(\mathbf{r}_0, \dots, \mathbf{r}_{P-1}) = (\pi \|\mathbf{R}\|)^{-P} \cdot e^{-P \cdot \text{tr}\{\mathbf{R}^{-1} \cdot \hat{\mathbf{R}}\}} \quad (19)$$

where  $\mathbf{r}_p$  is the receive vector at the moment of the  $p$ -th sample,  $\hat{\mathbf{R}}$  is estimate of the covariance matrix estimate over the samples, and  $\|\cdot\|$  and  $\text{tr}\{\cdot\}$  denote the determinant and trace operations, respectively.

From equation (19), it is readily found that the negative log-likelihood function of the sample vectors is

$$-\ln(\mathbf{L}) = N \cdot P \cdot \ln(\pi) + P \cdot \ln(\|\mathbf{R}\|) + P \cdot \text{tr}\{\mathbf{R}^{-1} \cdot \hat{\mathbf{R}}\}. \quad (20)$$

The Gaussianity of the error vector  $\mathbf{w}$  implies that the entries of the *Fisher Information Matrix*  $\mathbf{J}$ , from which the Cramer-Rao bounds is obtained, can be computed using the Slepian-Bang's formula below, [25]

$$\mathbf{J}_{i,j} = \text{tr}\{\mathbf{R}^{-1} \cdot \partial \mathbf{R} / \partial \eta_i \cdot \mathbf{R}^{-1} \cdot \partial \mathbf{R} / \partial \eta_j\}, \quad (21)$$

where the subscript  $i, j$  denotes the element on the  $i$ -th row (element) and  $j$ -th column of the corresponding matrix (vector).

The partial derivatives required to construct the Fisher Information Matrix are given by

$$\partial \mathbf{R} / \partial \sigma_w^2 = \mathbf{I}, \quad (22)$$

$$\partial \mathbf{R} / \partial \boldsymbol{\Gamma} = \mathbf{A} \cdot \mathbf{R}_s \cdot \boldsymbol{\Gamma}^T \cdot \mathbf{A}^T + \mathbf{A} \cdot \boldsymbol{\Gamma} \cdot \mathbf{R}_s \cdot \mathbf{A}^T, \quad (23)$$

$$\partial \mathbf{R} / \partial \boldsymbol{\tau} = \dot{\mathbf{A}}_{\boldsymbol{\tau}} \cdot \mathbf{R}_s \cdot \boldsymbol{\Gamma}^T \cdot \mathbf{A}^T + \mathbf{A} \cdot \boldsymbol{\Gamma} \cdot \mathbf{R}_s \cdot \dot{\mathbf{A}}_{\boldsymbol{\tau}}^T, \quad (24)$$

$$\partial \mathbf{R} / \partial \boldsymbol{\theta} = \dot{\mathbf{A}}_{\boldsymbol{\theta}} \cdot \mathbf{R}_s \cdot \boldsymbol{\Gamma}^T \cdot \mathbf{A}^T + \mathbf{A} \cdot \boldsymbol{\Gamma} \cdot \mathbf{R}_s \cdot \dot{\mathbf{A}}_{\boldsymbol{\theta}}^T, \quad (25)$$

$$\partial \mathbf{R} / \partial \boldsymbol{\phi} = \dot{\mathbf{A}}_{\boldsymbol{\phi}} \cdot \mathbf{R}_s \cdot \boldsymbol{\Gamma}^T \cdot \mathbf{A}^T + \mathbf{A} \cdot \boldsymbol{\Gamma} \cdot \mathbf{R}_s \cdot \dot{\mathbf{A}}_{\boldsymbol{\phi}}^T, \quad (26)$$

where  $\dot{\mathbf{A}}_{\boldsymbol{\tau}}$ ,  $\dot{\mathbf{A}}_{\boldsymbol{\theta}}$  and  $\dot{\mathbf{A}}_{\boldsymbol{\phi}}$  given by

$$\dot{\mathbf{A}}_{\boldsymbol{\tau}} = \partial \mathbf{A} / \partial \boldsymbol{\tau} = \begin{bmatrix} \frac{\partial R_{0,m_0}(\tau_0)}{\partial \tau_0} & \cdots & \frac{\partial R_{0,m_{K-1}}(\tau_{K-1})}{\partial \tau_{K-1}} \\ \vdots & \ddots & \vdots \\ \frac{\partial R_{N-1,m_0}(\tau_0 + \Delta \tau_{0,N-1})}{\partial \tau_0} & \cdots & \frac{\partial R_{N-1,m_{K-1}}(\tau_{K-1} + \Delta \tau_{K-1,N-1})}{\partial \tau_{K-1}} \end{bmatrix}, \quad (27)$$

$$\dot{\mathbf{A}}_{\boldsymbol{\theta}} = \partial \mathbf{A} / \partial \boldsymbol{\theta} = \mathbf{D} \cdot \dot{\mathbf{A}}_{\boldsymbol{\tau}} \odot \sin(\boldsymbol{\Theta}) \odot \cos(\boldsymbol{\Phi}), \quad (28)$$

$$\dot{\mathbf{A}}_{\boldsymbol{\phi}} = \partial \mathbf{A} / \partial \boldsymbol{\phi} = \mathbf{D} \cdot \dot{\mathbf{A}}_{\boldsymbol{\tau}} \odot \cos(\boldsymbol{\Theta}) \odot \sin(\boldsymbol{\Phi}), \quad (29)$$

where  $\odot$  denotes the Hadamard (element-by-element) product, and the matrices  $\mathbf{D}$ ,  $\boldsymbol{\Theta}$  and  $\boldsymbol{\Phi}$  are respectively given by

$$\mathbf{D} = \begin{bmatrix} d_0 & & \mathbf{0} \\ & \ddots & \\ \mathbf{0} & & d_{N-1} \end{bmatrix}, \quad (30)$$

$$\boldsymbol{\Theta} = \begin{bmatrix} \theta_0 - \vartheta_0 & \cdots & \theta_{K-1} - \vartheta_0 \\ \vdots & \ddots & \vdots \\ \theta_0 - \vartheta_{N-1} & \cdots & \theta_{K-1} - \vartheta_{N-1} \end{bmatrix}, \quad (31)$$

$$\boldsymbol{\Phi} = \begin{bmatrix} \phi_0 - \varphi_0 & \cdots & \phi_{K-1} - \varphi_0 \\ \vdots & \ddots & \vdots \\ \phi_0 - \varphi_{N-1} & \cdots & \phi_{K-1} - \varphi_{N-1} \end{bmatrix}. \quad (32)$$

The entries of the Fisher Information Matrix corresponding to each of the parameters  $\sigma_w^2$ ,  $\Gamma$ ,  $\tau$ ,  $\theta$  and  $\phi$  are computed from equations (21) through (32), and summarized as follows.

1) *Entry on the Noise Power:*

$$J_{\sigma_w^4} = \text{tr} \{ \mathbf{R}^{-2} \}. \quad (33)$$

2) *Entries on the Variance of Physical Parameters:*

$$J_{\eta_i^2} = \text{tr} \left\{ (\mathbf{R}^{-1} \cdot \partial \mathbf{R} / \partial \eta_i)^2 \right\}, \quad (34)$$

where  $\eta_i$  represents  $\Gamma$ ,  $\tau$ ,  $\theta$  or  $\phi$ , one at a time.

3) *Entries on the Covariance of Physical Parameters:*

$$J_{\eta_i \eta_j} = J_{\eta_j \eta_i} = \text{tr} \{ \mathbf{R}^{-1} \cdot \partial \mathbf{R} / \partial \eta_i \cdot \mathbf{R}^{-1} \cdot \partial \mathbf{R} / \partial \eta_j \}, \quad (35)$$

where  $\eta_i$  and  $\eta_j$  represent a mutually exclusive pair of the parameters  $\Gamma$ ,  $\tau$ ,  $\theta$  and  $\phi$ .

4) *Entries on the Covariance of a Physical Parameter with the Noise Power:*

$$J_{\sigma_w^2 \eta_i} = 0. \quad (36)$$

The Fisher Information Matrix then becomes,

$$\mathbf{J} = \begin{bmatrix} J_{\sigma_w^2} & \mathbf{0} \\ \mathbf{0} & \begin{matrix} J_{\Gamma^2} & J_{\Gamma\tau} & J_{\Gamma\theta} & J_{\Gamma\phi} \\ J_{\tau\Gamma} & J_{\tau^2} & J_{\tau\theta} & J_{\tau\phi} \\ J_{\theta\Gamma} & J_{\theta\tau} & J_{\theta^2} & J_{\theta\phi} \\ J_{\phi\Gamma} & J_{\phi\tau} & J_{\phi\theta} & J_{\phi^2} \end{matrix} \end{bmatrix} = \begin{bmatrix} J_{\sigma_w^2} & \mathbf{0} \\ \mathbf{0} & \tilde{\mathbf{J}} \end{bmatrix}. \quad (37)$$

Finally, the Cramer-Rao bound<sup>3</sup> on the parameter vector  $\boldsymbol{\eta}$  is given by,

$$\mathbf{C}(\boldsymbol{\eta}) = \mathbf{J}^{-1}. \quad (38)$$

The bound for the estimation error variance on the noise power  $\sigma_w^2$  can be easily computed from  $\mathbf{C}(\boldsymbol{\eta})$  using the bordering method [26], which reduces equation (38) to

$$C(\sigma_w^4) = \mathbf{C}_{1,1}(\boldsymbol{\eta}) = \left[ \begin{array}{c|c} J_{\sigma_w^2}^{-1} & \mathbf{0} \\ \hline \mathbf{0} & \tilde{\mathbf{J}}^{-1} \end{array} \right]_{1,1} = \frac{1}{J_{\sigma_w^2}}. \quad (39)$$

Although useful closed-form expressions for the bounds on the physical vector-parameters  $\Gamma$ ,  $\tau$ ,  $\theta$  and  $\phi$  cannot be obtained, efficient numerical computation can be performed using the Cramer's rule, which gives,

$$C(\eta_i) = \| [\mathbf{J}]_{i,i} \| \cdot \| \mathbf{J} \|^{-1}, \quad (40)$$

where  $[\mathbf{J}]_{i,j}$  denotes the so-called *cofactor* associated to the  $(i, j)$ -th entry of  $\mathbf{J}$ , defined as the matrix that results from  $\mathbf{J}$  when its  $i$ -th row and  $j$ -th column are deleted.

Making use of the following property in equation (40),

$$\det \left( \begin{bmatrix} \alpha & \mathbf{0} \\ \mathbf{0} & \mathbf{X} \end{bmatrix} \right) = \alpha \| \mathbf{X} \|, \quad (41)$$

we finally obtain,

$$C(\eta_i) = \| [\tilde{\mathbf{J}}]_{i,i} \| \cdot \| \tilde{\mathbf{J}} \|^{-1}. \quad (42)$$

<sup>3</sup>The formulation adopted here is such that the resulting Cramer-Rao bound is related to the estimates of the *set* of parameters (all sources). The formulation for each parameter considered individually is similar, only with the derivatives given by equations (33) through (35) taken element-by-element.

## V. NUMERICAL RESULTS

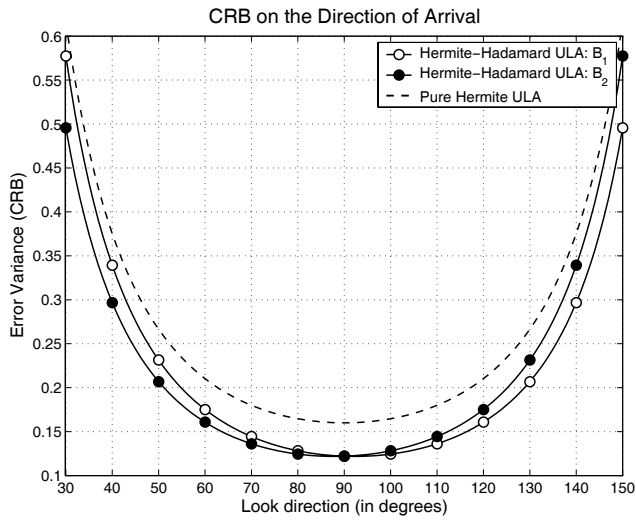
In this sub-section, the Cramer-Rao bounds derived above are utilized to compare the performances of the Hermite and the Hadamard arrays, with respect to the estimation of location parameters. Figure 2, for instance gives the Cramer-Rao bounds on the variances of DoA estimates obtained with 4-element uniform linear, rectangular, and spherical arrays. All results are obtained over 100 samples in a single source scenario using the first Hermite wavelet as incoming signal and under perfect synchronization conditions ( $\tau = 0$ ), and the coefficient matrices used in all plots are obtained through the numeric optimization described in section III.

Note that since none of the correlation filters employed in the elements of a Hadamard array is matched to the incoming waveform, the total energy collected by these arrays are, in fact, less than that collected by a Hermite array with the same structure. Therefore, for a fair comparison, the signal-to-noise-ratio figure is defined as the ratio between the energy of the incoming pulse and the total noise at the output of the array (denoted  $\text{SNR}_{\text{in/out}}$ ). All results are for  $\text{SNR}_{\text{in/out}} = 10\text{dB}$ , which is rather low, considering that the array receiver is correlation-based [17]. The figure not only shows that optimized Hadamard arrays are superior to Hermite arrays, but also illustrates the relationship between the apparent size of an array and the corresponding expected performances in the estimation of positioning parameters.

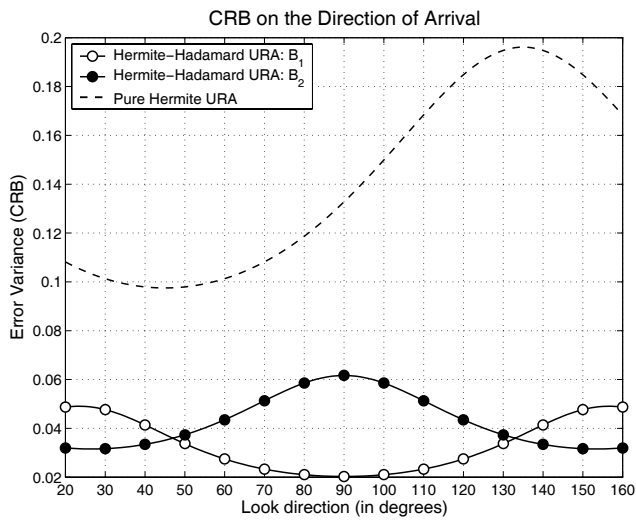
Next, in figure 3, the Cramer-Rao bounds on the variances of TDoA estimates using the two different array constructions are compared. Three sub-figures are given, each corresponding to incoming pulses at a different incidence angle. The array antenna is a three-dimensional tetrahedric array and all the remaining conditions are the same as those assumed previously. It is again found that the results obtained with the Hadamard arrays are generally better than those achieved with Hermite arrays. More importantly, it is seen that although the coefficient matrices obtained as described in section III are not generally optimum<sup>4</sup>, it yields near-optimum results over a significantly wide span of the domain. Comparing figures 2 and 3, it is also noticeable that the Cramer-Rao bounds on the TDoA estimates are much lower than those on the DoA estimates, indicating that the optimization process of section III is indeed adequate.

Finally, the performances of the Hermite and the Hadamard arrays in the estimation of positioning parameters in a scenario with two correlated sources are compared in figure 4. The signals of both sources are assumed to have equal energy (normalized to the unity) and impinge from different directions. Curves corresponding to the Hermite array are shown in dashed lines. Results corresponding to Hadamard arrays with coefficient matrices given by mutually exclusive permutations of the 4-by-4 Hadamard matrix are shown with dotted lines, and the results obtained with optimized coefficient matrices appear detached, in solid lines with markers. Since the Cramer-Rao bounds are related to the performance of the Maximum Likelihood estimator, the figure provides evidence that array antennas with Hermite-Hadamard orthogonal correlation filters in their elements can (at least theoretically) handle the presence of correlated and even coherent signals.

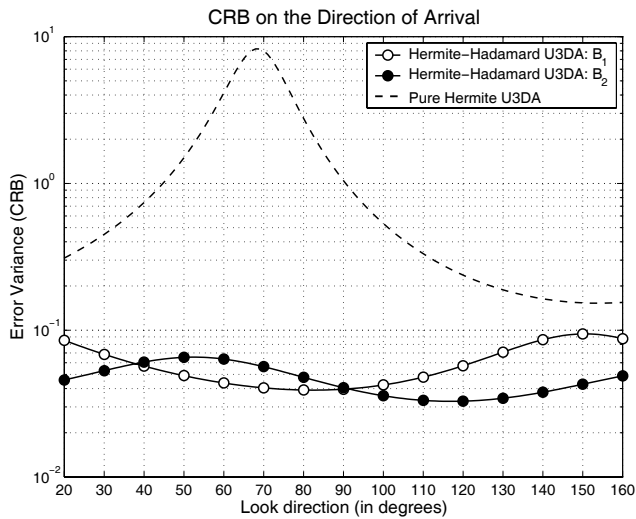
<sup>4</sup>The existence of a globally optimal solution for the coefficient matrix is rather unlikely.



(a) Uniform Linear Array (Length =  $\lambda$ ,  $N = Q = 4$ )

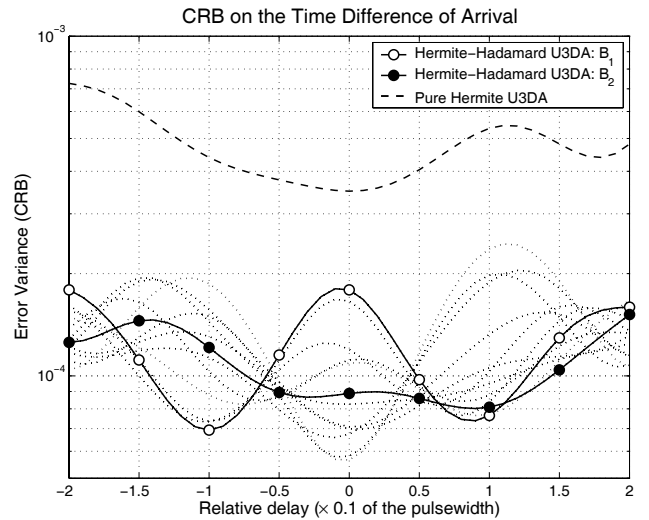


(b) Uniform Rectangular Array (Length =  $\lambda$ ,  $N = Q = 4$ )

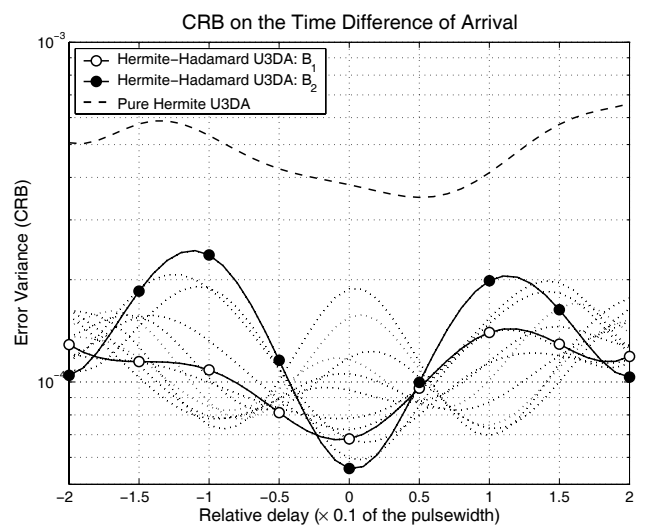


(c) Uniform Spherical Array (Length =  $\lambda$ ,  $N = Q = 4$ )

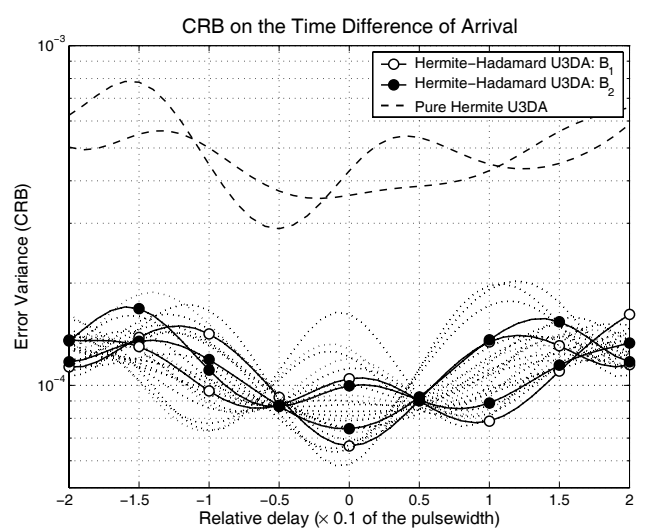
Fig. 2. Cramer-Rao Bounds on the variances of DoA estimation errors with Hermite and Hermite-Hadamard arrays.



(a) Incidence angles ( $\theta = 0^\circ$ ,  $\phi = 0^\circ$ )

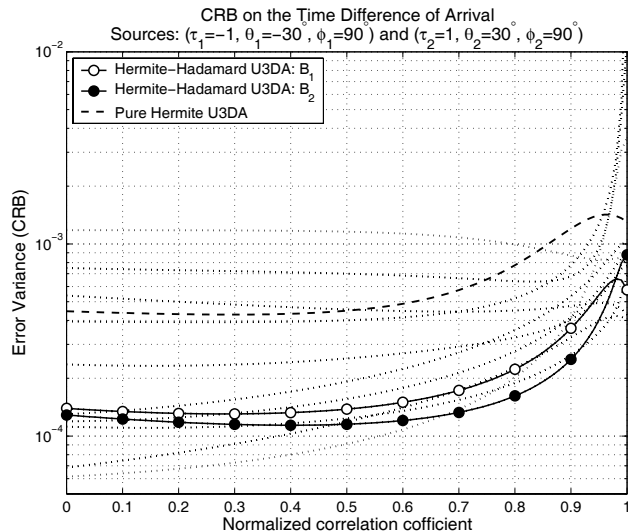


(b) Incidence angles ( $\theta = 90^\circ$ ,  $\phi = 0^\circ$ )

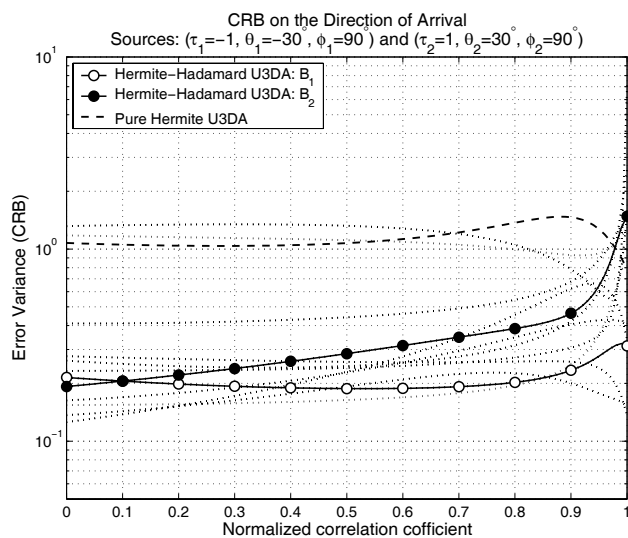


(c) Incidence angles ( $\theta = 90^\circ$ ,  $\phi = 90^\circ$ )

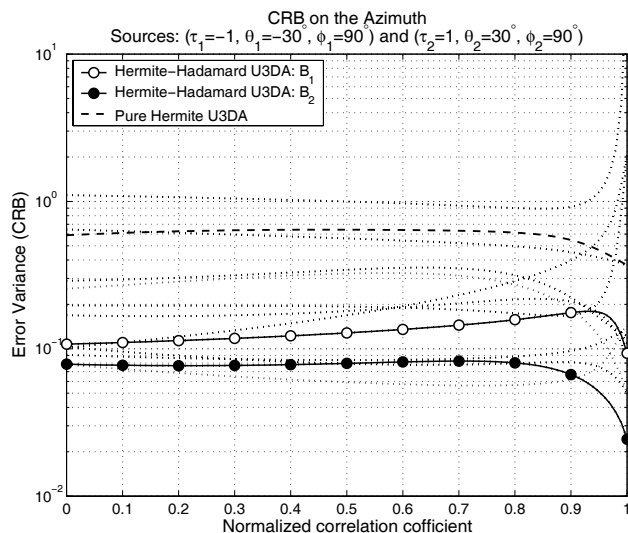
Fig. 3. Cramer-Rao Bounds on the variances of DoA estimation errors with Hermite and Hermite-Hadamard arrays.



(a)  $CRB(\tau|\theta, \phi)$



(b)  $CRB(\theta|\tau, \phi)$



(c)  $CRB(\phi|\tau, \theta)$

Fig. 4. Cramer-Rao Bounds on the for the estimates of  $\tau$ ,  $\theta$  and  $\phi$  with a U3DA as a function of the source correlation coefficient.

## REFERENCES

- [1] G. Su and M. Morf, "The signal subspace approach for multiple wide-band emitter location," *IEEE Trans. Acoust., Speech, Signal Processing*, vol. 31, no. 6, pp. 1502 – 1522, Dec. 1983.
- [2] H. Wang and M. Kaveh, "Coherent signal-subspace processing for the detection and estimation of angles of arrival of multiple wide-band sources," *IEEE Trans. Acoust., Speech, Signal Processing*, vol. 33, no. 4, pp. 823 – 831, Aug. 1985.
- [3] Y. Grenier, "Wideband source location through frequency-dependent modeling," *IEEE Trans. Signal Processing*, vol. 42, no. 5, pp. 1087 – 1096, May 1994.
- [4] A. Belouchrani and M. G. Amin, "Time-frequency MUSIC," *IEEE Signal Processing Lett.*, vol. 6, no. 5, pp. 109–110, May 1999.
- [5] A. Gershman and M. Amin, "Wideband direction-of-arrival estimation of multiple chirp signals using spatial time-frequency distributions," *IEEE Signal Processing Lett.*, vol. 7, pp. 152 – 155, June 2000.
- [6] M. G. M. Hussain, "Principles of space-time array processing for ultrawide-band impulse radar and radio communications," *IEEE Trans. Veh. Technol.*, vol. 51, pp. 393 – 403, May 2002.
- [7] T. Sato, G. Abreu, and R. Kohno, "Beamforming array antenna with heterogeneous signal distribution for uwb pulse transmission," *IEICE Transactions on Fundamentals of Electronics, Communications and Computer Sciences - Special Issue on Wideband Systems*, vol. J86-A, no. 12, pp. 1302 – 1309, Dec. 2003.
- [8] H. Krim and M. Viberg, "Two decades of array signal processing research: the parametric approach," *IEEE Signal Processing Mag.*, vol. 13, no. 4, pp. 67 – 94, July 1996.
- [9] R. J.-M. Cramer, R. A. Scholtz, and M. Z. Win, "Evaluation of an ultra-wide-band propagation channel," *IEEE Trans. Antennas Propagat.*, vol. 50, no. 5, pp. 561 – 570, May 2002.
- [10] A. H. Nayfeh and D. T. Mook, *Nonlinear Oscillations*. New York, NY: John Wiley & Sons, 1979.
- [11] K. Marsden, H. J. Lee, D. S. Ha, and H. S. Lee, "Low power cmos re-programmable pulse generator for uwb systems," in *Proc. IEEE Conference on Ultra Wideband Systems and Technologies (UWBST) - (UWBST'03)*, Reston, USA, Nov. 16–19, 2003, pp. 443–447.
- [12] S. Bagga, W. A. Serdijn, and J. R. Long, "A ppm gaussian monocycle transmitter for ultra-wideband communications," in *International Workshop on Ultra Wideband Systems (IWUWBS) Joint with Conference on Ultra Wideband Systems and Technologies (UWBST) - (Joint UWBST & IWUWBS'04)*, Kyoto, Japan, May 18–21, 2004, pp. 130–134.
- [13] L. E. Miller, "Models for uwb pulses and their effects on narrowband direct conversion receiver," in *Proc. IEEE 2<sup>nd</sup> Ultra Wideband Systems and Technologies (UWBST'03)*, Reston, VA, U.S.A., Nov. 16-19 2003.
- [14] G. Abreu, T. Uefuji, and R. Kohno, "Parameter estimation of uwb-ir signals using array antennas with hermite-hadamard orthogonal filters," in *Proc. IEEE 7<sup>th</sup> Wireless Personal Multimedia Conference (WPMC'04)*, Abano Terme, Italy, Sept. 12-15 2004, pp. 288–292.
- [15] A. D. Poularikas, *The Transforms and Applications Handbook, Second Edition*, 2nd ed. CRC Press, Feb.23 2000.
- [16] G. Abreu, "Closed-form correlation functions of generalized hermite wavelets," *IEEE Trans. Signal Processing*, 2004, to appear.
- [17] M. Z. Win and R. A. Scholtz, "Ultra-wide bandwidth time-hopping spread-spectrum impulse radio for wireless multiple-access communications," *IEEE Trans. Commun.*, vol. 48, pp. 679 – 691, Apr. 2000.
- [18] H. L. Van-Trees, *Optimum Array Processing (Detection, Estimation, and Modulation Theory, Part IV)*, 1st ed. New York, N.Y.: Wiley-Interscience, Mar.22 2002.
- [19] G. Bienvenu and L.Kopp, "Optimality of high resolution array processing using the eigensystem approach," *IEEE Trans. Acoust., Speech, Signal Processing*, vol. 31, no. 5, pp. 1235 – 1248, Oct. 1983.
- [20] H. Wang and M. Kaveh, "On the performance of signal-subspace processing—part ii: Coherent wide-band systems," *IEEE Trans. Acoust., Speech, Signal Processing*, vol. 35, no. 11, pp. 1583 – 1591, Nov. 1987.
- [21] J. G. Proakis, *Digital Communications, Fourth Edition*. New York, NY: Mc-Graw-Hill, 2000.
- [22] G. Abreu, C. J. Mitchell, and R. Kohno, "Jitter-robust orthogonal hermite pulses for ultra wideband impulse radio communications," *EURASIP Journal on Applied Signal Processing*, no. 3, pp. 369 – 381, Mar. 2005.
- [23] S. N. Batalama and D. Kazakos, "On the generalized cramer-rao bound for the estimation of the location," *IEEE Trans. Signal Processing*, vol. 45, no. 2, pp. 487 – 492, Feb. 1997.
- [24] N. R. Goodman, "Statistical analysis based on a certain multivariate complex gaussian distribution," *Annals Math. Stat.*, vol. 34, pp. 152 – 177, 1963.
- [25] P. Stoica and R. L. Moses, *Introduction to Spectral Analysis*, 1st ed. Englewood Cliffs, New Jersey: Prentice Hall, Feb.6 1997.
- [26] J. R. Westlake, *A Handbook of Numerical Matrix Inversion and Solution of Linear Equations*. New York, NY: John Wiley & Sons, 1968.